

Short communication

Exploring highly energetic quaternary double transition metal MAX phase M_2ScSiC_2 ($M = Ti$, and V) compositions along with *ab-initio* assessments

Ahmed Azzouz-Rached^{a,*}, Mostafa Azzouz-Rached^b, Nasir Rahman^{c,*}, Mudasser Husain^l, Nourreddine Sfina^d, Vineet Tirth^{e,f}, Ali Bentouaf^g, Md Ferdous Rahman^h, Norah Algethamiⁱ, Hanan A. Althobaiti^j, Khamael M. Abualnaja^k, Ghaida Alosaimi^k

^a Magnetic Materials Laboratory, Faculty of Exact Sciences, Djillali Liabes University of Sidi Bel-Abbes, Algeria^b Faculty of Exact Sciences and Informatics, Hassiba Benbouali University of Chlef, Algeria^c Department of Physics, University of Lakki Marwat, 28420, Lakki Marwat, Khyber Pakhtunkhwa, Pakistan^d College of Sciences and Arts in Mahayel Asir, Department of Physics, King Khalid University, Abha, Saudi Arabia^e Mechanical Engineering Department, College of Engineering, King Khalid University, Abha 61421, Asir, Kingdom of Saudi Arabia^f Research Center for Advanced Materials Science (RCAMS), King Khalid University, Guraiger, P.O. Box 9004, Abha-61413, Asir, Kingdom of Saudi Arabia^g Communication Technology Laboratory, Faculty of Technology, Dr. Moulay, Tahar University of Saida, 20000 Saida, Algeria^h Advanced Energy Materials and Solar Cell Research Laboratory, Department of Electrical and Electronic Engineering, Begum Rokeya University, Rangpur 5400, Bangladeshⁱ Department of Physics, Faculty of Science, Taif University, P.O. Box 11099, Taif 21944, Saudi Arabia^j Physics Department, College of Science, Taif University, P.O. Box 11099, Taif 21944, Saudi Arabia^k Department of Chemistry, Faculty of Science, Taif University, Taif 21944, Saudi Arabia^l State Key Laboratory for Mesoscopic Physics and Department of Physics Peking University Beijing 100871, PR China

ARTICLE INFO

ABSTRACT

Keywords:

DFT investigations
312-MAX phases
Structural properties
Thermodynamic characteristics
Mechanical characteristics
Thermal barrier coatings

Recently, MAX phases have garnered significant technological interest due to their unique combination of ceramic and metallic properties. In this research, we utilized the full potential linearized augmented plane wave (FP-LAPW) technique to comprehensively investigate the mechanical, structural, electrical, and thermodynamic characteristics of M_2ScSiC_2 ($M = Ti$, V). Our findings indicate that the α -polymorph structures of these compounds are more stable than the β -polymorph structures at ground state. Notably, calculations of formation energy, elastic constants (Cij), and phonon band structures confirm that these compounds are thermodynamically and mechanically stable. We found that M_2ScSiC_2 ($M = Ti$, V) exhibit a brittle nature. The high melting points and Debye temperatures of these compounds make them well-suited for applications in hostile environments, such as thermal barrier coatings. Furthermore, an examination of the electronic structure confirmed their metallic behavior. Additionally, we explored thermodynamic characteristics, such as heat capacity at the Debye temperature and constant volume, over a temperature range of 0 to 1500 K and under high-pressure conditions from 0 to 30 GPa. We anticipate that this research will inspire further experimental and theoretical investigations into these materials' properties within the MAX phase community worldwide.

1. Introduction

Recently, the MAX phase has become the center of attention in the cutting-edge world due to its impressive combination of thermal and mechanical characteristic at high pressure and high temperatures, as well as its unique blend of ceramic and metallic characteristic [1–3].

Regarding this matter, the MAX phase exhibits numerous prospective uses. These include its role as high-temperature and high-pressure heating elements, durable and easily machinable refractories capable of withstanding thermal shocks, components for nuclear applications that can endure neutron irradiation, coatings for electrical connections, a precursor for generating carbide-derived carbon, and as a source

* Corresponding authors.

E-mail addresses: a.azzouzrached@univ-chlef.dz (A. Azzouz-Rached), mostaphaazzouz02@gmail.com (M. Azzouz-Rached), nasir@ulm.edu.pk (N. Rahman), 2201110247@stu.pku.edu.cn (M. Husain), nsfina@kku.edu.sa (N. Sfina), vtirth@kku.edu.sa (V. Tirth), lilo.btf@gmail.com (A. Bentouaf), ferdousapee@gmail.com (Md Ferdous Rahman), algethami80@gmail.com (N. Algethami), h.althubaity@tu.edu.sa (H.A. Althobaiti).

material for producing MXenes, which are a category of two-dimensional materials comprising Transition metal nitride, carbide, boride, and carbonitride formulations [4–7].

The MAX phases represent a family of stratified ternary compounds, consisting of transition metals denoted as “M,” group (13)–(16) elements identified as “A,” and either carbon, nitrogen, or boron labeled as “X.” These compounds follow a general formula, $M_{n+1}AX_n$, where “n” can take on values of 1, 2, or 3. These compounds are renowned for their exceptional properties, [8,9]. The MAX phases can be categorized into three subsets based on the layer index “n”: M_2AX ($n = 1$), M_3AX_2 ($n = 2$), and M_4AX_3 ($n = 3$), which are also commonly known as 211, 312, and 413 MAX phases, respectively. In the context of the $M_{n+1}AX_n$ crystal structure, the $M_{n+1}X_n$ ceramic layers are typically separated by a spotless metallic A layer. This arrangement results in the presence of mixed bonds, where the M (metallic)-X (covalent) bonds exhibit remarkable strength, while the M (metallic)-A (metallic) bonds are comparatively weaker [10]. Consequently, $M_{n+1}AX_n$ phases possess an exceptionally low friction coefficient, making them highly amenable to processing [11,12]. These exceptional properties have positioned $M_{n+1}AX_n$ phases as highly sought-after materials in an extensive array of industrial and technological uses such as the nuclear industry, wear- and corrosion-resistant coatings, Li-ion batteries, electrodes, spintronics, and superconducting materials [13–18]. In recent times, Mn + 1AXn phases have gained prominence as superior and more suitable options for potential structural applications in nuclear reactions, owing to their distinctive attributes. Given their intriguing and exceptional properties, $M_{n+1}AX_n$ phase materials are currently the subject of extensive experimental and theoretical investigations. Researchers are also meticulously focused on enhancing the range and effectiveness of $M_{n+1}AX_n$ phase materials to meet specific requirements [19]. These investigations may cover a range of facets, such as the identification of novel Mn + 1AXn phases and the integration of those already known [20–22]. Consequently, many researchers have recently dedicated their efforts to exploring the elastic, mechanical, electrical, optical, and other physical characteristics of materials using density functional theory (DFT) approaches to uncover their full potential [23–25]. Transition elements-based alloys offer advantageous properties that find wide-ranging benefits across aerospace, automotive, and biomedical sectors [26–31]. The composition and characteristics of the MAX phases can be modified and enhanced by introducing additional elements into their crystal lattice. These results in isostructural MAX phase compounds. The past few years have seen an increasing concentrate on these mixed solutions as a means to improve the attributes of MAX phases. For example, the addition of Al on the A-site or Nb on the M–site to Ti_3SiC_2 leads to the formation of $Ti_3(Si_{1-x}Al_x)C_2$ or $(Nb_{1-x}Ti_x)_3SiC_2$ solid solutions, which are found to be more oxidation-resistant [32,33]. Meng et al. [34] and Barsoum et al. [35] discussed the effect of solid solution hardening for $(V_xTi_{1-x})_2AlC$ and $Ti_2AlC_xN_y$, respectively, while Bei et al. [36] reported a solid solution softening effect for $Ti_3(Al_{1-x}Sn_x)C_2$. Incorporating Ti into the M–site of Nb_4AlC_3 to a certain extent notably enhances the mechanical characteristics, including Vickers hardness, fracture toughness, and flexural strength [37,38]. The variation in the x-content within $Cr_2-xMxGeC$ (where M can be Ti, V, Mn, Fe, or Mo) influences the thermal, electrical, magnetic, and structural transport attributes [39]. Introducing Zirconium (Zr), Hafnium (Hf), and Niobium (Nb) as solid solutions, with partial incorporation, enhances the elastic moduli and robustness of Ti_3SiC_2 , especially when exposed to higher temperatures [40]. The addition of Silicon (Si) to Ti_3AlC_2 leads to a substantial enhancement in both Young’s and shear moduli [41]. Based on a theoretical investigation, the introduction of Ti atoms in Zr_3AlC_2 , to a certain extent, improves its mechanical strength [42]. Recently, Anasori et al. [43] discovered two novel compounds MAX phases, Mo_2TiAlC_2 and $Mo_2Ti_2AlC_3$. Fu et al., clarified the arrangement of Mo and Ti atomic layers within the crystal structure. Additionally, they achieved the successful production of a highly pure, compact $Mo_2Ti_2AlC_3$ specimen with a relative density of 99.3 % through the application of the hot-

pressing technique. They conducted an in-depth examination of its mechanical and physical properties [44]. According to Fu et al., the $Mo_2Ti_2AlC_3$ ceramic exhibits the least heat-conductive of all the MAX phases that are currently known, measuring 6.82 W/(m·K). The studies by M. Bendjemai et al and I. Ouadha et al. on the quaternary MAX phases M_2ScSnC_2 , and Mn_2VSnC_2 , respectively, have shown that these compounds are stable both dynamically and mechanically [45,46]. Despite extensive research on quaternary MAX phases, researchers continue to explore new compounds in search of optimal physical properties. Many key characteristics, including structural, mechanical, electrical, phase stability, and thermodynamic characteristics, remain uncertain. To our best knowledge, there was no extensive research on the technologically important mechanical properties of M_2ScSiC_2 ($M = Ti$, and V). Herein, due to finding out the alternative of quaternary double transition metal MAX phases MAX phases for photovoltaic and optoelectronic implementation, we used density functional theory [47,48] based on fundamental principles to determine the mechanical, electrical, and optical characteristics of M_2ScSiC_2 ($M = Ti$, and V) MAX phases. In our calculations, we utilized the full potential linearized augmented plane wave (FP-LAPW) technique, renowned for its high precision in calculating electronic structures, especially for materials with complex crystal structures like MAX phases. This method divides space into non-overlapping muffin-tin spheres centered at atomic sites and an interstitial region, allowing for accurate treatment of both core and valence electrons. Additionally, FP-LAPW is versatile, applicable to a wide range of materials including metals, semiconductors, and insulators. This versatility is crucial for studying MAX phases, which exhibit a combination of metallic and ceramic characteristics. Furthermore, FP-LAPW is highly effective in calculating elastic constants and phonon dispersion relations, essential for assessing the mechanical stability and vibrational properties of materials.

2. Theoretical methods

The data examined in this study was obtained employing the full-potential linearized augmented plane wave approach [49–51], which employs all electrons and is run on the WIEN2K code [52]. DFT is the foundation of this method, which uses the Perdew-Burke-Ernzerhof generalized gradient approximations (PBE-GGA) [53] to analyze physical properties. The muffin-tin (MT) radii parameters selected for different atoms are as follows: 1.98 (Ti), 1.94 (V), 2.3 (Sc), 2.1 (Si), and 1.62 Bohr (C). The maximum charge density within the atomic spheres is specified as $l_{max} = 10$, and the charge density Fourier expansion employs the largest vector $G_{max} = 14$. To ensure reliable convergence, the energy and charge criteria for convergence are set at less than 10⁻⁵ Ry and 10⁻⁴ e/a.u.3, respectively. Additionally, integration over the Brillouin zone (BZ) is performed employing an $11 \times 11 \times 4$ Monkhorst-Pack k-point grid.

3. Results and discussion

In this section provides a detailed presentation and discussion of the findings from studying the different physical properties of M_2ScSiC_2 .

3.1. Structural characteristics and stability

The hexagonal structure of M_2ScSiC_2 has a space group of P6₃/mmc (No. 194) and is composed of layers [54]. The positions of Ti/V, Sc, Si, and C atoms in the quaternary MAX phase were assessed using the Wyckoff notations of 2a, 4f, 2d, and 4f, while the specific atomic coordinates within the crystal lattice are detailed in Table 1. In the M_2ScSiC_2 compounds, the unit cell contains generally twelve atoms which is presented in Fig. 1. Furthermore, Fig. 2 illustrates the relationship between total energy and volume for both compounds, each of which can exist in two distinct structures, referred to as the α -polymorph and β -polymorph. The information unequivocally demonstrates that the

Table 1
displays the Wyckoff placements for the presently recognized polymorphs.

<u>Atom</u> α -polymorph	<u>Site</u>	<u>Coordinates</u>				Z_i -range
		Wyckof	x	y	z	
M _I (Sc)	4f		0	0	0
M _{II} (Ti/V)	2a		1	2	Z_M	$0.13725730^1/0.14220575^2$
			3	3		
A(Si)	2d		0	0	$\frac{1}{4}$
X(C)	4f		$\frac{2}{3}$	$\frac{1}{3}$	Z_C	$0.08077278^1/0.08365340^2$
			$\frac{3}{3}$	$\frac{3}{3}$		
β -polymorph	Wyckof		x	y	z	Z_i -range
	4f		0	0	0
	2a		1	2	Z_M	$0.12165934^1/0.12496869^2$
			3	3		
	2d		$\frac{1}{3}$	$\frac{2}{3}$	$\frac{1}{4}$
	4f		$\frac{2}{3}$	$\frac{1}{3}$	Z_C	$0.07454467^1/0.077725965^2$
			$\frac{3}{3}$	$\frac{3}{3}$		

¹ Ti_2ScSiC_2 ² V_2ScSiC_2 .

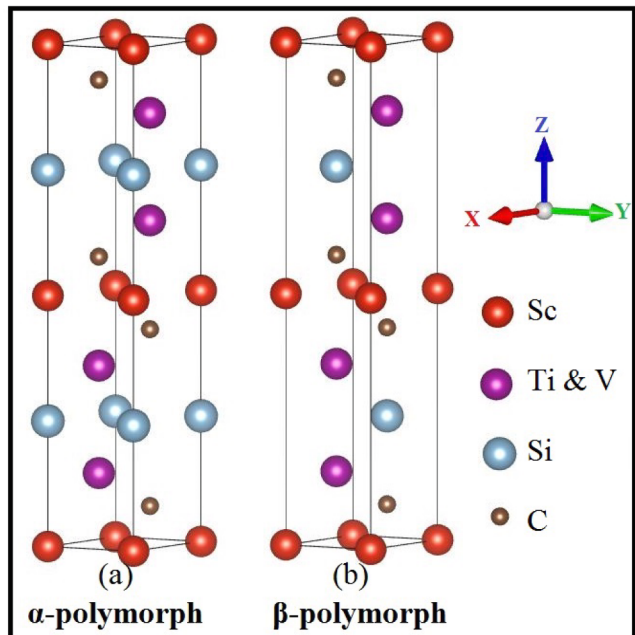


Fig. 1. A view of the crystal structure of the 2112 MAX phases.

α -polymorph has less overall energy than the β -polymorph, signifying its greater stability and equilibrium lattice parameters [55,56]. The Table 2 lists its optimized cell parameters. We conclude that our results are in excellent agreement with the results for the MAX phase's family.

Before commencing the calculation of the physical properties, we ensured the accuracy of the energy of formation, which is widely regarded as a dependable indicator of compound stability. In this case, we used the following equation to calculate the formation energy [57]:

$$E_{Form}^{M2ScSiC_2} = \frac{E_{total}^{M2ScSiC_2} - aE_{tot}^M - bE_{tot}^S - cE_{tot}^C - dE_{tot}^C}{a + b + c + d} \quad (1)$$

Here, $E_{Form}^{M2ScSiC_2}$ represents the formation energy of M_2ScSiC_2 , with M being either Ti or V. E_{tot} denotes the overall energy of the bulk chemicals per unit cell, where atoms 'a', 'b', 'c', and 'd' stand for the atom counts of M, Sc, Si, and C, in that order. Our results, as recorded in Table 2, indicate that the formation energy values are negative, confirming the thermodynamic stability of all our compounds. Furthermore, we verified the stability of these compounds in the Open Quantum Materials

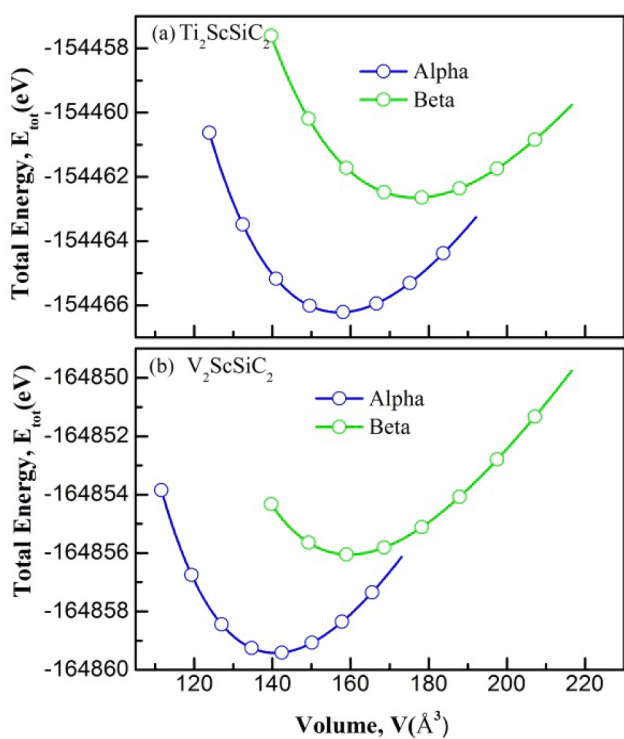


Fig. 2. Fluctuations in energy relative to volume in our compounds.

Database (OQMD). Subsequently, we calculated phonon frequencies and dispersion curves using the linear response method and the super-cell methodology. Phonon dispersion curves are the most reliable indicators of compound stability. Fig. 3 illustrates the resulting phonon scattering curves. The absence of imaginary frequencies in the positive phonon dispersion curves, as presented in Fig. 3, signifies the absence of negative dispersion curves. To our knowledge, no measurements or calculations have been conducted for the formation energy and phonon dispersion curves of M_2ScSiC_2 compounds. As a result, our findings can be regarded as a quantitative theoretical forecast.

3.2. Mechanical properties

To project the stability of our compounds MAX phases, five related elastic constants for a hexagonal crystal, such as C_{11} , C_{12} , C_{13} , C_{33} , C_{44} and C_{66} , have been investigated precisely using Hex-elastic package. In general, the calculated elastic constants should satisfy the following Born stability requirement to be mechanically stable. Thus, for a hexagonal phase, the Born stability criteria are specified as follows [58]:

$$\begin{cases} C_{11} > |C_{12}|, 2C_{13}^2 < (C_{11} + C_{12})C_{33} \\ C_{44} > 0, C_{66} > 0 \end{cases} \quad (2)$$

Following that, Table 3 lists the values of the elastic constants. The M_2ScSiC_2 satisfies the above-Born stability criteria i.e. five single elastic constants fulfil these criteria, demonstrating this is a mechanical stable. It is ubiquitously known that Cauchy pressure for two different directions for a hexagonal structure, and typically demonstrates the difference between C_{13} , C_{44} , and C_{12} , C_{66} , respectively, and its positive and negative value indicates the ductile and brittle nature [9,45,46]. Herein, we found only a negative value of Cauchy pressure, signifying the brittle nature of Ti_2ScSiC_2 and V_2ScSiC_2 . The Cauchy pressure can also function as a determinant for discerning whether a material is characterized by covalent or ionic bonds. Negative Cauchy pressure is linked to covalent bonds, whereas positive Cauchy pressure indicates the presence of ionic bonds. It's worth noting that compounds Ti_2ScSiC_2 and V_2ScSiC_2 exhibit

Table 2

Provides the computed lattice parameters, bulk modulus (B), pressure derivative of the bulk modulus (B'), internal parameters c/a ratio [z (M) and z (X)], formation energy E_{form} (eV/atom), and total energy E_{tot} (eV).

Parameters	Ref	Phase	a (Å)	c (Å)	c/a	Z_M	Z_C	B (GPa)	B'	E_{form} (eV/atom)	E_{tot} (eV)
$\text{Ti}_2\text{ScSiC}_2$	Our work	Alpha	3.15	18.27	5.80	0.13725730	0.08077278	170.25	4.0	-1.023	-154466.233
		Beta	3.18	20.12	6.32	0.12165934	0.07454467	142.45	3.9	-1.542	-154462.663
V_2ScSiC_2		Alpha	3.03	17.58	5.78	0.14220575	0.08365340	200.27	4.0	-0.856	-164859.436
		Beta	3.08	19.36	6.27	0.12496869	0.07772596	169.21	4.2	-1.056	-164856.059

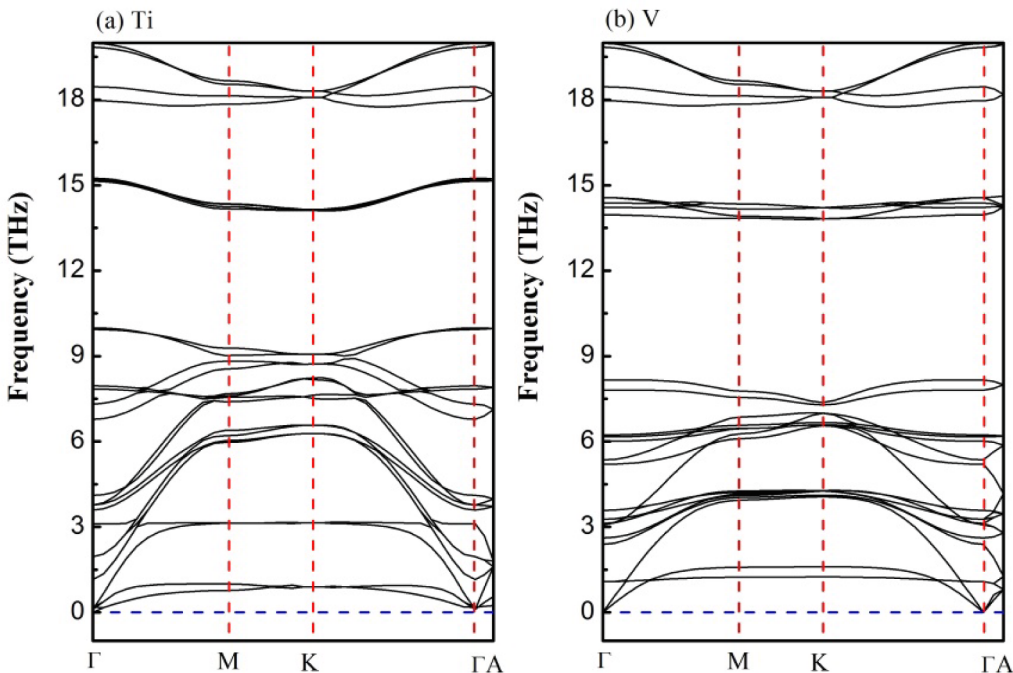


Fig. 3. The calculated phonons dispersion in the first Brillouin zone for quaternary $M_2\text{ScSiC}_2$ ($M = \text{Ti}, \text{V}$) with the high symmetries axes.

Table 3

Computed elastic constants (C_{ij}) in (GPa) and the Cauchy pressure for two distinct directions across our mixtures.

Compound	Ref	C_{11}	C_{33}	C_{12}	C_{13}	C_{55}	C_{66}	P_X^{Cauchy}	P_Z^{Cauchy}
$\text{Ti}_2\text{ScSiC}_2$	Our work	312	337	90	98	134	111	-36	-25
V_2ScSiC_2		332	373	107	135	170	112	-34	-04

covalent bonds. As for now, the current findings concerning the elastic constants reveal an interesting distinction between three compounds, where we see clearly that C_{11} surpasses C_{33} , signifying that compressing along the a and b -axes is more challenging than along the c -axis. Furthermore, it is important to highlight that in all of our compounds, both the C_{11} and C_{33} elastic constants exhibit considerably greater values compared to the remaining elastic constants, leading to a notable degree of elastic anisotropy within these materials. Moreover, upon contrasting the C_{13} and C_{66} values across all our compounds, it becomes apparent that shear deformation, as denoted by C_{66} , is more prone to occur when subjected to shear stresses along the horizontal [100] direction within the vertical {100} plane.

However, using the Voigt-Reuss-Hill (VRH) equating methodology, the polycrystalline elastic moduli of $M_2\text{ScSiC}_2$ ($M = \text{Ti}, \text{V}$, and Cr) and the Poisson's ratio, have been computed. Any hexagonal crystal's Voigt and Reuss constraints on B and G have been determined using these formulas [59]:

$$B_V = \frac{1}{2}(2(C_{11} + C_{12}) + 4C_{13} + C_{33}) \quad (3)$$

$$G_V = \frac{1}{30}(C_{11} + C_{12} + 2C_{33} - 4C_{13} + 12C_{44} + C_{66}) \quad (4)$$

Reuss's approximation [60]

$$B_R = \frac{(C_{11} + C_{12})C_{33} - 2C_{13}^2}{C_{11} + C_{12} + 2C_{33} - 4C_{13}} \quad (5)$$

$$G_R = \frac{5}{20} \times \frac{C_{44}C_{66}[(C_{11} + C_{12})C_{33} - 2C_{13}^2]}{3B_V C_{44}C_{66} + \{(C_{11} + C_{12})C_{33} - 2C_{13}^2\}(C_{44} + C_{66})} \quad (6)$$

Hill's approximation [61]

$$B_H = \frac{(B_V + B_R)}{2} \quad (7)$$

$$G_H = \frac{(G_V + G_R)}{2} \quad (8)$$

By using the bulk modulus and shear modulus, the following are the values of Young's modulus (E) and Poisson's ratio (ν):

$$E = \frac{9BG}{3B + G} \quad (9)$$

$$\nu = \frac{3B - 2G}{2(3B + G)} \quad (10)$$

The computed bulk modulus predominantly characterizes size-related elasticity, whereas the shear modulus quantifies the material's resilience to shape-related deformation. Additionally, the shear modulus acts as a signal of a material's hardness by reflecting its resistance to plastic deformation under shear stress [62]. The computed results for the polycrystalline elastic modulus can be found in Table 4. As stated in Table 4, it clearly indicates that the bulk modulus (B) significantly surpasses the shear modulus (G), i.e., $B > G$. This distinction suggests that the shear modulus is the preferred descriptor for characterizing the stability of M_2ScSiC_2 . Moreover, a lower value of shear modulus (G) in comparison to the bulk modulus (B) indicates heightened resistance to volume distortion under the influence of outside pressure, signifying a more covalent nature in the atomic bonds [63]. Pugh [64] introduced the B/G ratio as a metric for assessing material ductility. When comparing this ratio to a critical threshold that distinguishes between ductile and brittle behavior, it becomes evident that the B/G values for both compounds fall short of the threshold of 1.75, indicating that these materials exhibit brittle characteristics. In contrast, we can consider Poisson's coefficient (ν) as an indicator of brittleness, adhering to Frantsevich's rule. When ν values exceed 0.26, it signifies ductility [65]. In the case of both compounds, their ν values less than 0.26, which unequivocally confirms their brittle characteristics.

Typically, mechanical properties are linked to the bulk and shear moduli of materials, collectively referred to as hardness. The Vicker's hardness H_V is computed here by using the empirical formula, where $k = G/B$ [66].

$$H_V = 2(K^2G)^{0.585} - 3 \quad (11)$$

The hardness values are measured at 19 GPa for Ti_2ScSiC_2 and 18 GPa for V_2ScSiC_2 . It's evident that our compounds are significantly harder than others compounds, signifying that our compounds exhibits greater hardness. Both values, however, fall within the typical hardness range for MAX phases [67].

While shear anisotropic factors play a crucial role in evaluating the anisotropy in atomic bonding across distinct planes, their significance becomes evident in various physical phenomena. Some of these phenomena include the development of plastic deformation in materials and the formation of micro-scale cracks in ceramics. The subsequent equations are employed to calculate anisotropic shear factors A_1 , A_2 , and A_3 for MAX phases [68].

$$A_1 = \frac{(C_{11} + C_{12} + 2C_{33} - 4C_{13})}{6C_{55}} \quad (12)$$

$$A_2 = \frac{2C_{55}}{(C_{11} - C_{12})} \quad (13)$$

$$A_3 = A_1 \cdot A_2 = \frac{(C_{11} + C_{12} + 2C_{33} - 4C_{13})}{3(C_{11} - C_{12})} \quad (14)$$

Subsequently, the linear compressibility coefficients can be acquired using the equation that follows [69]:

Table 4

Presents elastic modulus (B, E and G) measured in (GPa), the B/G ratio, Poisson's ratio and Vickers hardness.

Compounds	Ref	B	G	B/G	E	H_V	ν
Ti_2ScSiC_2	Our work	170	120	1.41	293	19	0.213
V_2ScSiC_2		198	131	1.51	323	18	0.228

$$\frac{k_c}{k_a} = \frac{(C_{11} + C_{12} - 2C_{13})}{(C_{33} - C_{13})} \quad (15)$$

The anisotropy factor is a widely recognized indicator of the degree of elastic anisotropy within a crystal. When equals 1, it signifies that the compound is entirely isotropic. A high A_i value, when applying tangential force to screw dislocations, can accelerate the cross-slip pinning process. As demonstrated in Table 5, the calculated anisotropy factors for both compounds differ from 1, providing additional confirmation of their elastic anisotropy behavior, and for the linear compressibility coefficients, we have seen that the is smaller than 1, showing that the compressibility along the 'a' and 'b' axes is greater than that along the 'c' axis.

3.3. Thermal properties

Both science and technology have a vested interest in investigating the thermal properties under high-temperature and high-pressure conditions. Critical thermal parameters under scrutiny encompass the minimal thermal conductivity, melting point, Debye temperature, and lattice thermal conductivity of M_2ScSiC_2 compound. The Debye temperature (θ_D) serves as a versatile parameter for characterizing a material's physical features, encompassing specific heat, melting point, lattice vibrations, thermal expansion, and thermal conductivity. Additionally, it holds relevance in the realms of superconductors, where it is connected to both the superconducting transition temperature and the electron-phonon coupling constant. Anderson's suggested average sound velocity can be employed to compute the Debye temperature and is interconnected with the elastic modulus as follows [70]:

$$\theta_D = \frac{\hbar}{k_B} \left[\frac{3n}{4\pi} \left(N_A \cdot \frac{\rho}{M} \right) \right]^{\frac{1}{3}} \cdot v_m \quad (16)$$

Where '' is Planck's constant, '' N_A denotes Avogadro's number, and 'n' represents the number of atoms. Additionally, the average velocity can be expressed as the following:

$$v_m = \left[\frac{1}{3} \left(\frac{2}{v_t^3} + \frac{1}{v_l^3} \right) \right]^{\frac{-1}{3}} \quad (17)$$

The v_l and v_t correspond to the transverse as well as longitudinal sound velocities, which are expressed in terms of the B and G as

$$v_l = \left(\frac{3B + 4G}{3\rho} \right)^{\frac{1}{2}} \quad (18)$$

$$v_t = \left(\frac{G}{\rho} \right)^{\frac{1}{2}} \quad (19)$$

The calculated θ_D along with sound wave velocities v_l , v_t and v_m are listed in Table 6. Both Ti_2ScSiC_2 and V_2ScSiC_2 possess high sound wave velocities and high Debye temperatures, which qualify them for usage in harsh situations.

Additionally, we looked into the melting temperature (T_m) of solid solutions involving M_2ScSiC_2 . The melting temperature is a parameter commonly used to assess the purity of both organic and inorganic compounds. To calculate T_m , an empirical formula based on elastic

Table 5

Displays the computed shear anisotropic parameters for the three different shear planes (A_1 , A_2 and A_3) and.. K_c/K_a

Parameters	Ref	A_1	A_2	A_3	K_c/K_a
Ti_2ScSiC_2	Our work	0.85	1.16	0.99	0.89
V_2ScSiC_2		0.63	1.51	0.95	0.71

Table 6

Calculated average elastic wave velocity, density, and transverse, longitudinal waves [ρ (in g/cm³), v_l , v_t , v_m (in m/s)] the lowest and lattice thermal conductivity at 300 K (k_{min} , k_{ph} in W/m-K), the melting temperature (T_m in K), and the Debye temperatures (θ_D in K).

Parameters		ρ (g/cm ³)	v_l	v_t	v_m	θ_D	T_m	k_{min}	k_{ph}
Ti ₂ ScSiC ₂	Our work	4.0764	9019.45	5442.61	6017.48	760.182	1825	1.14	48.73
V ₂ ScSiC ₂		4.6961	8923.68	5291.95	5860.76	768.064	1911	1.19	45.24

constants established for hexagonal crystals by Fine et al. has been employed [71]:

$$T_m = 354 + \frac{3}{2}(2C_{11} + C_{33}) \quad (20)$$

In Table 6, you can find the anticipated melting temperatures for the solid solutions involving M₂ScSiC₂. It is evident that T_m decreases as the concentration of M decreases. In fact, when V is completely substituted with Ti, T_m is reduced by 5 %. The solid solutions of M₂ScSiC₂ should be promising structural materials for application in thermally hostile environments due to their elevated melting temperatures.

Lattice thermal conductivity stands as a fundamental property of solids. Regarding MAX phases, which possess partial ceramic characteristics, the Slack model offers a suitable framework for determining lattice thermal conductivity [72]. This model considers the average number of atoms (M/n) within a 'molecule,' which is equivalent to the atoms present in the crystal's formula unit, along with their average atomic mass. It serves as a valuable tool for assessing the temperature-dependent lattice thermal conductivity of materials, employing the following equation:

$$k_{ph} = A \frac{M_{av} \theta_D^3 \delta}{\gamma^2 n^{2/3} T} \quad (21)$$

In this equation, M_{av} represents the average atomic mass per mole in kilograms, θ_D is the Debye temperature in Kelvin, n represents the number of atoms in a standard unit cell, and δ is the cubic root of the average atomic volume in meters. T stands for the temperature in Kelvin, and γ is the Grüneisen parameter. The Grüneisen parameter can be derived from the Poisson's ratio using the given equation:

$$\gamma = \frac{3(1 + \nu)}{2(2 - 3\nu)} \quad (22)$$

The factor $A(\gamma)$ attributed to Julian [63] can be obtained as

$$A(\gamma) = \frac{5.720 \times 10^7 \times 0.849}{2 \times \left(1 - \frac{0.514}{\gamma} + \frac{0.228}{\gamma^2}\right)} \quad (23)$$

The lattice thermal conductivity values for Ti₂ScSiC₂ and V₂ScSiC₂ at room temperature (300 K) are detailed in Table 6. It's important to note that lattice thermal conductivity is notably influenced by the Debye temperature. The reliability of the Slack model for MAX phases is well-supported, given that the computed lattice thermal conductivity closely aligns with experimental data. For example, at 1300 K, the experimental lattice thermal conductivity for Ta₄AlC₃ and Nb₄AlC₃ is 5 (6) W/m-K and 7 (7) W/m-K, respectively [73]. The lattice thermal conductivity for Ti₂ScSiC₂ and V₂ScSiC₂ MAX phases, computed under ambient pressure and temperature conditions, stands at 18.8 and 19.2 W/m-K, respectively. These values fall within the typical range for MAX phases [74]. The Fig. 4 shows how the lattice thermal conductivity of M₂ScSiC₂ gradually decreases as temperature rises under various pressures.

The lowest achievable thermal conductivity (k_{min}) signifies the theoretical lower boundary of a material's inherent thermal conductivity at elevated temperatures. At elevated temperatures, phonons no longer remain paired, causing the transfer of heat to adjacent atoms. In this scenario, we can estimate the average distance between neighboring atoms as the mean free path of phonons. Using this approximation,

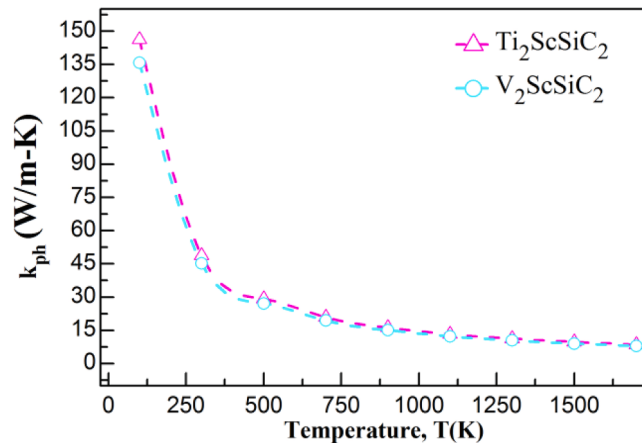


Fig. 4. Displays the relationship between temperature and the lattice thermal conductivity of the M₂ScSiC₂ (M = Ti, V) compounds.

various atoms in a molecule can be substituted by an 'equivalent atom' with an average atomic mass of M/n, where n denotes the number of atoms in a primitive cell. It's essential to emphasize that a 'single equivalent atom' within the cell does not exhibit optical modes. Drawing upon this concept, Clarke introduced a method for calculating the thermal conductivity at high temperatures in his model [75].

$$k_{min} = k_B v_m \left(\frac{n N_A \rho}{M} \right) \quad (24)$$

The symbols employed in Equation (16) carry the identical significance as those employed in this equation. The two MAX phases' lowest thermal conductivity, Ti₂ScSiC₂ and V₂ScSiC₂, is presented in Table 6. Notably, the lowest possible thermal conductivity values for our compounds are in line with the exceptionally low minimal thermal conductivity of 1.25 W/m-K, commonly utilized in the selection of suitable components of the thermal barrier coating (TBC) applications [76]. Consequently, M₂ScSiC₂ emerges as a potential candidate for TBC materials.

3.4. Electronic properties

Understanding the electronic characteristics of materials is fundamental to gaining meaningful insights into their properties and behavior. In our analysis, we initiated by computing the band structure of specific compounds under investigation, focusing particularly on critical points within the initial Brillouin zone (BZ). This initial step allows us to discern the energy bands and their dispersion, providing essential information about the materials' electronic behavior.

The results of the band structure analysis, as depicted in Fig. 5, reveal a notable topological similarity among the band structures of the quaternary MAX phases under scrutiny. These graphical representations illustrate significant dispersion within both the valence and conduction bands. Notably, we observe a considerable overlap between the valence and conduction bands at the Fermi level across all considered compounds, indicating their metallic nature. Subsequently, we conducted a comprehensive analysis of the projected density of states (PDOS) and total density of states (TDOS) over an extensive energy range symmetrically centered around the Fermi level. Fig. 6 illustrates the TDOS and

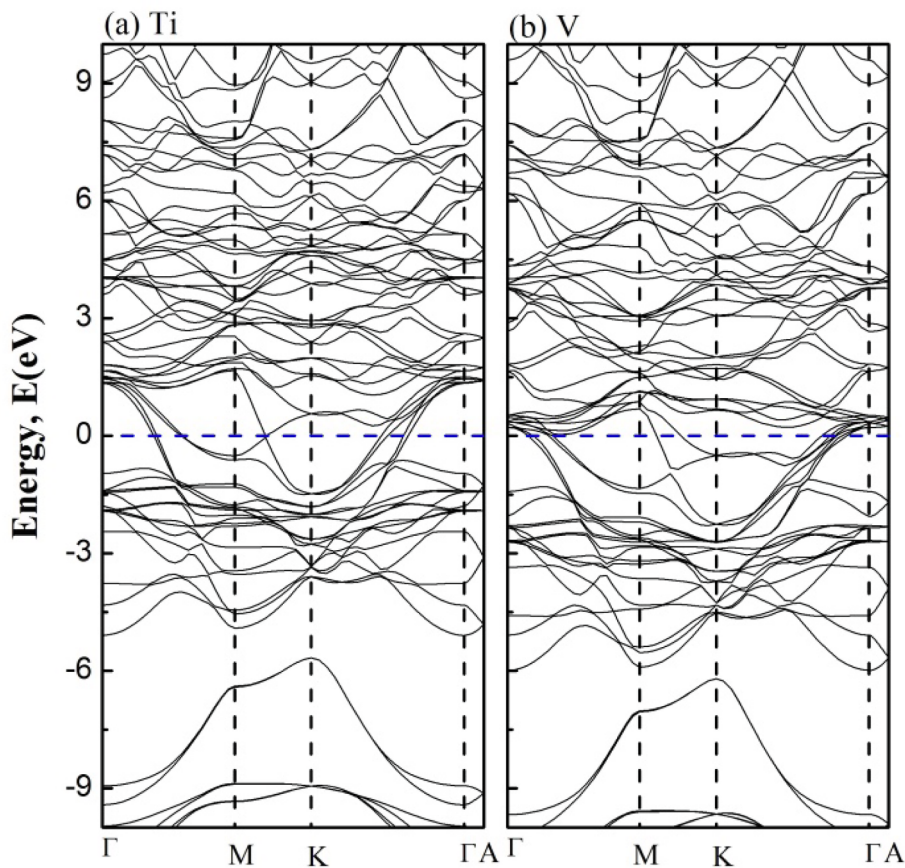


Fig. 5. Band structure of the $M_2\text{ScSiC}_2$ ($M = \text{Ti}$ & V) compounds within the high-symmetry directions of the initial Brillouin zone.

PDOS plots for $M_2\text{ScSiC}_2$ ($M = \text{Ti}, \text{V}$). The persistent non-zero value in the TDOS at the Fermi level provides compelling evidence for the metallic nature of these compounds, attributed to the transitional properties of Ti and V. Further examination of the PDOS data allows us to categorize the density of states spectrum into three primary regions. Firstly, in the lower valence band region, we observe noticeable s-s hybridization between the s and p orbitals of the C and Si atoms. Secondly, in the vicinity of the Fermi level, there is a significant overlap between the d orbitals of M and the p orbitals of Si/C, indicating substantial covalent bonding in $\text{Ti}_2\text{ScSiC}_2$ and V_2ScSiC_2 . Finally, in the remaining region, there is a reduced degree of covalent bonding between the d orbitals of M/Sc and the p orbitals of Si/C.

3.5. Thermodynamic properties

In this study, we have examined the fundamental thermodynamic properties, like lattice parameters, that are crucial for our research, Debye temperature, heat capacity at constant volume, and the thermal expansion coefficient to justify the excellence of $M_2\text{ScSiC}_2$ in high mechanical applications. These parameters are calculated and discussed here up to 1500 °K of temperatures and 30GPa to pressures are explored to study the properties of thermodynamics. Using the quasi-harmonic Debye model in conjunction with the Gibbs package [77]. This rigorous examination allows us to gain profound insights into how materials respond and adapt to the unique conditions encountered in these hostile environments. Fig. 7 represents the variation of Volume (V) according to pressure and temperature. It is evident that as temperature fluctuates under specific pressures, the volume steadily rises. In contrast, the volume has experienced a notable decrease at a constant temperature with increasing pressure. Under ambient conditions (300 K and 0 GPa), the volumes of $M_2\text{ScSiC}_2$ ($M = \text{Ti}, \text{V}$) discovered to be 1074.072

Bohr^3 and 961.644 Bohr^3 , respectively. Fig. 8 displays the heat capacity (C_V) of $M_2\text{ScSiC}_2$ ($M = \text{Ti} & \text{V}$) as functions of pressure and temperature. As temperature increases, C_V also rises. At lower temperatures, this increase is particularly pronounced, primarily attributable to the exponential growth in the number of excited phonon modes. Eventually, C_V stabilizes at higher temperatures, approximating the classical asymptotic limit known as the Dulong-Petit limit, where $C_V \approx 3n\text{NkB}$, approximately 296 J/mol K. Consequently, C_V follows the Debye T^3 power-law at lower temperatures, and at higher temperatures, the influence of anharmonicity on C_V is restricted.

Fig. 9 illustrates the result of pressure and temperature on the Debye temperature (θ_D) of $\text{Ti}_2\text{ScSiC}_2$ and V_2ScSiC_2 . At constant temperature, both phases exhibit an accelerated increase in θ_D as pressure rises. The Debye temperature serves as a gauge of crystal bonding strength. Notably, as temperature rises, atomic vibrations weaken the interatomic bonds, causing a corresponding decrease in θ_D . Conversely, pressure exerts an opposite effect; as it increases, θ_D rises swiftly at a given temperature due to enhanced bonding forces between atoms. The reduction in θ_D with temperature change is gradual, whereas the ascent in θ_D with pressure change is steep. Consequently, the influence of pressure on θ_D in $\text{Ti}_2\text{ScSiC}_2$ and V_2ScSiC_2 is more significant than that of temperature. Fig. 10 illustrates the result of pressure and temperature on the coefficient of thermal expansion. It's worth noting that, under constant pressure conditions, the coefficient of thermal expansion exhibits a rapid increase up to 300 K. Beyond this temperature threshold, a gradual and moderate increase in thermal expansion is observed, indicating a low temperature dependence of the coefficient at higher temperatures. Additionally, when pressure is applied, the thermal expansion coefficient of both MAX phases, $\text{Ti}_2\text{ScSiC}_2$ and V_2ScSiC_2 , shows a nearly linear decrease across the entire pressure range.

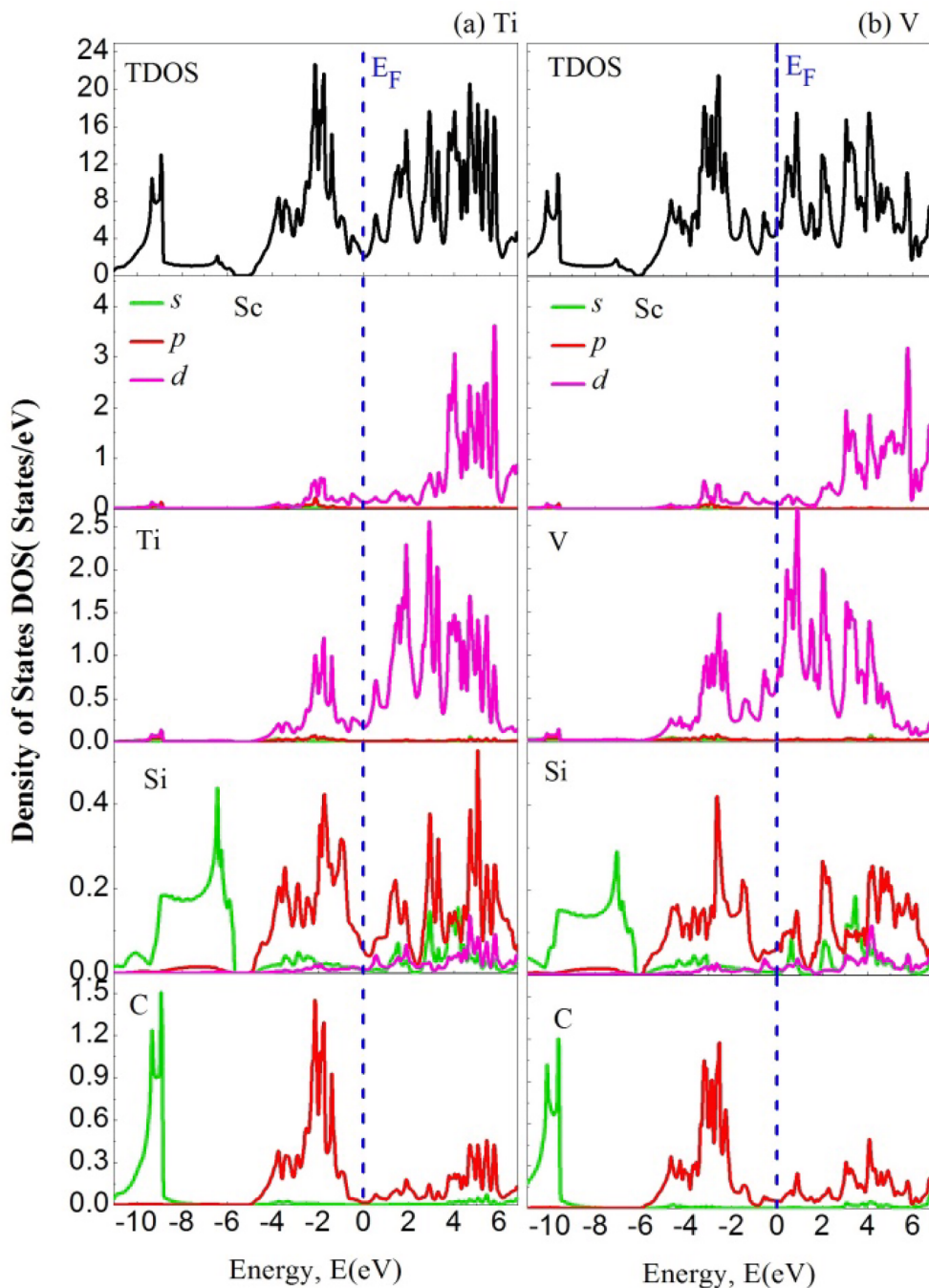


Fig. 6. Electronic densities of states of M_2ScSiC_2 ($M = Ti \& V$) compounds.

4. Conclusions

A theoretical investigation into the physical properties of two quaternary MAX phases, namely Ti_2ScSiC_2 and V_2ScSiC_2 , was conducted. Our analysis confirms the thermodynamic, mechanical, and dynamic stability of Ti_2ScSiC_2 and V_2ScSiC_2 , based on formation energy, elastic constants, and phonon band structures. The Cauchy pressure, Pugh's ratio, and Poisson's ratio indicate that both compounds exhibit brittleness and anisotropic behavior. Additionally, the band structures and density of states reveal metallic behavior in both materials, with significant overlap between the valence and conduction bands at the Fermi level. Our assessments indicate that owing to their elevated melting temperature and minimal thermal conductivity, these compounds hold promise for application in challenging conditions and as effective

thermal barrier coatings. Based on the aforementioned findings, it's evident that these quaternary MAX phases have promising applications in advanced energy technologies and other demanding applications.

5. Declarations

The authors declare that they have no conflict of interest.

Author contribution

Ahmed Azzouz-Rached, Mostafa Azzouz-Rached, Nasir Rahman, Mudasser Husain, Nourreddine Sfina, Vineet Tirth, Ali Bentouaf, wrote the manuscript. Hamza Rekab-Djabri, Norah Algethami, Hanan A. Althobaiti, khamael M. Abualnaja and GhaidaAlosaimi prepared

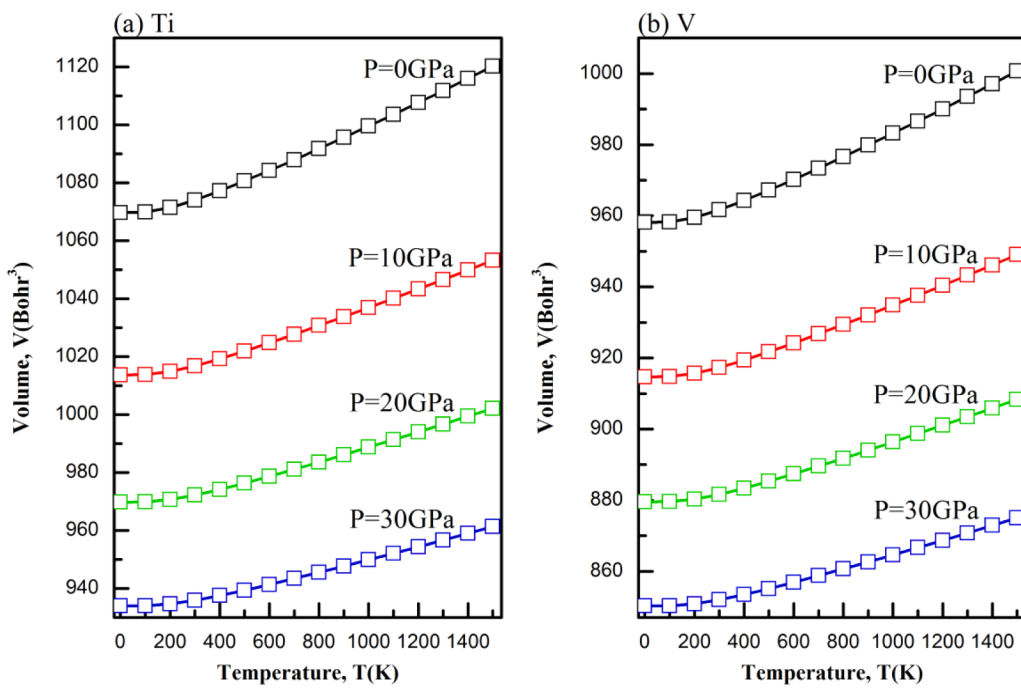


Fig. 7. Shows how the volume changes with temperature under various pressure conditions for the M_2ScSiC_2 ($\text{M} = \text{Ti}, \text{V}$) compounds.

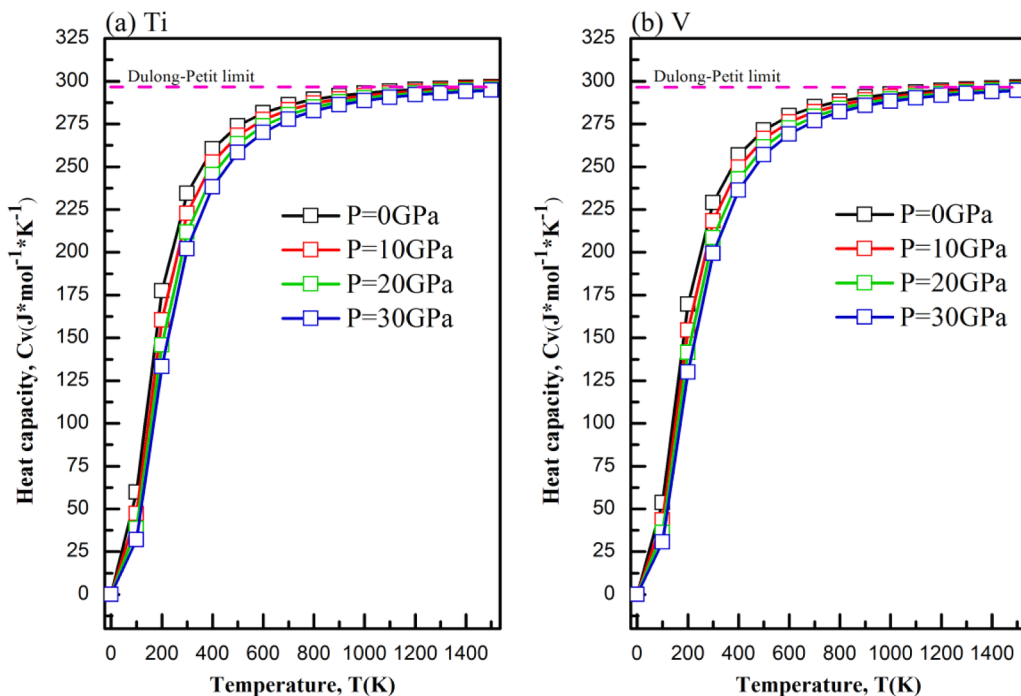


Fig. 8. The graph shows the variation of heat capacity (C_v) with temperature at different pressures for the M_2ScSiC_2 ($\text{M} = \text{Ti}, \text{V}$) compounds.

Figures.

All the authors reviewed the manuscript.

CRediT authorship contribution statement

Ahmed Azzouz-Rached: Data curation. **Mostafa Azzouz-Rached:** Data curation. **Nasir Rahman:** Supervision, Project administration, Conceptualization. **Mudasser Husain:** Formal analysis. **Nourreddine Sfina:** Methodology. **Vineet Tirth:** Software, Formal analysis. **Ali Bentouaf:** Validation. **Md Ferdous Rahman:** Investigation. **Norah**

Algethami: Visualization. **Hanan A. Althobaiti:** Investigation. **Khamael M. Abualnaja:** Validation. **Ghaida Alosaimi:** Validation.

Declaration of competing interest

The authors declare that they have no known competing financial interests or personal relationships that could have appeared to influence the work reported in this paper.

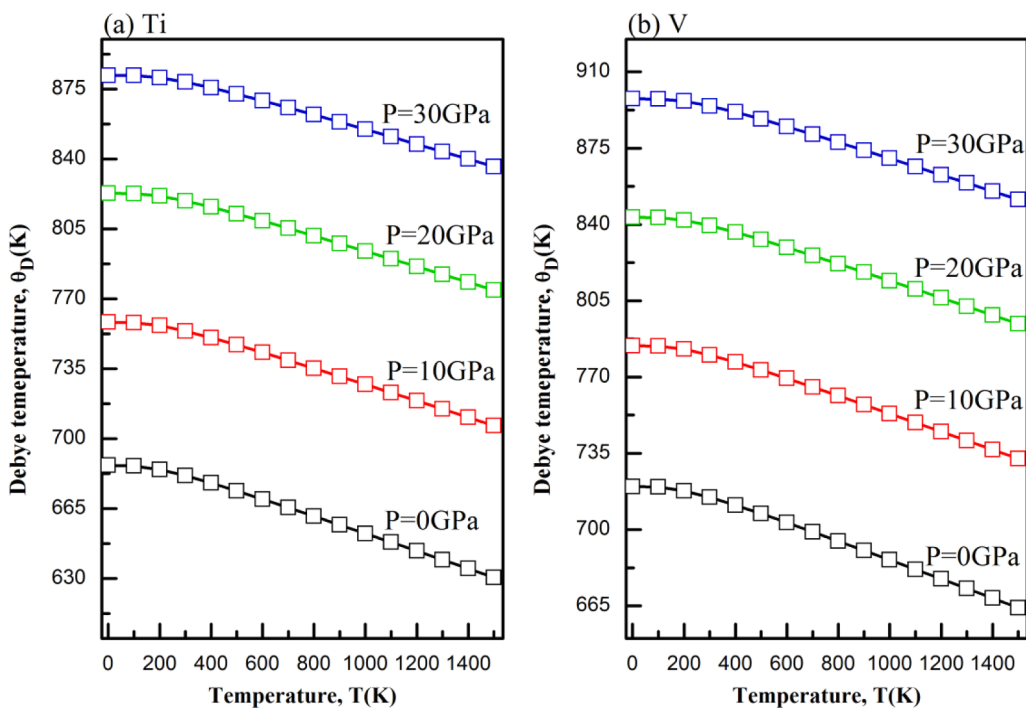


Fig. 9. The variation of the Debye temperature (θ_D) with temperature at different pressures for the $M_2\text{ScSiC}_2$ ($M = \text{Ti}, \text{V}$) compounds.

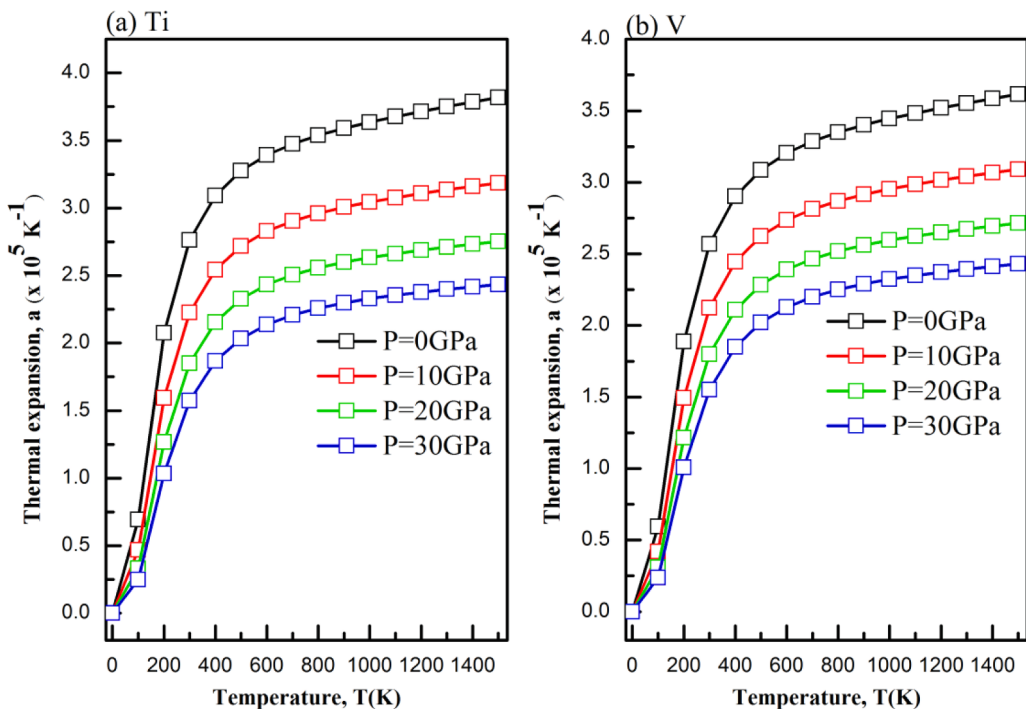


Fig. 10. illustrates how the thermal expansion coefficient varies with temperature at different pressure for the $M_2\text{ScSiC}_2$ ($M = \text{Ti}, \text{V}$) compounds.

Data availability

Data will be made available on request.

Acknowledgement

The authors extend their appreciation to the Deanship of Scientific Research at King Khalid University Abha 61421, Asir, Kingdom of Saudi Arabia for funding this work through the Large Groups Project under

grant number RGP. 2/545/44.

References

- [1] A. Azzouz-Rached, H. Rached, I. Ouadha, D. Rached, A. Reggad, The Vanadium-Doping Effect on Physical Properties of the Zr_2AlC MAX Phase Compound, *Mater. Chem. Phys.* 260 (2021) 124189.
- [2] M.W. Barsoum, MAX Phases: Properties of Machinable Ternary Carbides and Nitrides, John Wiley & Sons, 2013.

- [3] I. Ouadha, H. Rached, A. Azzouz-Rached, A. Reggad, D. Rached, Study of the Structural, Mechanical and Thermodynamic Properties of the New MAX Phase Compounds (Zr_1-XTix) $3AlC_2$, *Comput. Condens. Matter* 23 (2020) e00468.
- [4] Y. Kato, J.L. Snead, T. Cheng, C. Shih, W.D. Lewis, T. Koyanagi, T. Hinoki, C. H. Henager Jr, M. Ferraris, Radiation-Tolerant Joining Technologies for Silicon Carbide Ceramics and Composites, *J. Nucl. Mater.* 448 (1–3) (2014) 497–511.
- [5] A. Azzouz-Rached, M.A. Hadi, H. Rached, T. Hadji, D. Rached, A. Bouhemadou, Pressure Effects on the Structural, Elastic, Magnetic and Thermodynamic Properties of Mn_2AlC and Mn_2SiC MAX Phases, *J. Alloys Compd.* 885 (2021) 160998.
- [6] T. Zhu, H. Ding, C. Wang, Y. Liu, S. Xiao, G. Yang, B. Yang, Parameters Calibration of the GISSMO Failure Model for SUS301L-MT, *Chinese J. Mech. Eng.* 36 (1) (2023) 20.
- [7] J. Gonzalez-Julian, T. Go, D.E. Mack, R. Vaßen, Thermal Cycling Testing of TBCs on Cr_2AlC MAX Phase Substrates, *Surf. Coatings Technol.* 340 (2018) 17–24.
- [8] A. Azzouz-Rached, H. Rached, M.H. Babu, T. Hadji, D. Rached, Prediction of Double Transition Metal ($Cr_1 - XZrx$) $2AlC$ MAX Phases as Thermal Barrier Coatings: Insight from Density Functional Theory, *Int. J. Quantum Chem.* 121 (20) (2021) e26770.
- [9] Azzouz-Rached, A.; Qureshi, M. W.; Ouadha, I.; Rached, H.; Hadji, T.; Rebak-Djabri, H. DFT Analysis of Physical Properties of Quaternary MAX Phase Nitrides: $(Fe_0.5Mo_0.5)2SiN$ ($M = Cr \& Mn$). *Comput. Condens. Matter* 2022, 33, e00748.
- [10] P. Eklund, M. Beckers, U. Jansson, H. Höglberg, L. Hultman, The $Mn_1 + 1AlXn$ Phases: Materials Science and Thin-Film Processing, *Thin Solid Films* 518 (8) (2010) 1851–1878.
- [11] S. Gupta, D. Filimonov, V. Zaitsev, T. Palanisamy, T. El-Raghy, M.W. Barsoum, Study of Tribofilms Formed during Dry Sliding of Ta_2AlC/Ag or Cr_2AlC/Ag Composites against Ni-Based Superalloys and Al_2O_3 , *Wear* 267 (9–10) (2009) 1490–1500.
- [12] M. Rester, J. Neidhardt, P. Eklund, J. Emmerlich, H. Ljungcrantz, L. Hultman, C. Mitterer, Annealing Studies of Nanocomposite Ti–Si–C Thin Films with Respect to Phase Stability and Tribological Performance, *Mater. Sci. Eng. A* 429 (1–2) (2006) 90–95.
- [13] J. Xu, M.-Q. Zhao, Y. Wang, W. Yao, C. Chen, B. Anasori, A. Sarycheva, C.E. Ren, T. Mathis, L. Gomes, Demonstration of Li-Ion Capacity of MAX Phases, *ACS Energy Lett.* 1 (6) (2016) 1094–1099.
- [14] C. Lange, M.W. Barsoum, P. Schaaf, Towards the Synthesis of MAX-Phase Functional Coatings by Pulsed Laser Deposition, *Appl. Surf. Sci.* 254 (4) (2007) 1232–1235.
- [15] I.R. Shein, A.L. Ivanovskii, Elastic Properties of Superconducting MAX Phases from First-principles Calculations, *Phys. Status Solidi* 248 (1) (2011) 228–232.
- [16] J. Wang, Z. Liu, H. Zhang, J. Wang, Tailoring Magnetic Properties of MAX Phases, a Theoretical Investigation of (Cr_2Ti) AlC_2 and Cr_2AlC , *J. Am. Ceram. Soc.* 99 (10) (2016) 3371–3375.
- [17] D.W. Clark, S.J. Zinkle, M.K. Patel, C.M. Parish, High Temperature Ion Irradiation Effects in MAX Phase Ceramics, *Acta Mater.* 105 (2016) 130–146.
- [18] C. Zuo, C. Zhong, Screen the Elastic and Thermodynamic Properties of MAX Solid Solution Using DFT Procedue: Case Study on (Ti_1-XV_x) $2AlC$, *Mater. Chem. Phys.* 250 (2020) 123059.
- [19] G. Surucu, Investigation of Structural, Electronic, Anisotropic Elastic, and Lattice Dynamical Properties of MAX Phases Borides: An Ab-Initio Study on Hypothetical M_2AB ($M = Ti, Zr, Hf; A = Al, Ga, In$) Compounds, *Mater. Chem. Phys.* 203 (2018) 106–117.
- [20] D. Horlait, S.C. Middleburgh, A. Chroneos, W.E. Lee, Synthesis and DFT Investigation of New Bismuth-Containing MAX Phases, *Sci. Rep.* 6 (1) (2016) 18829.
- [21] P. Eklund, M. Dahlqvist, O. Tengstrand, L. Hultman, J. Lu, N. Nedfors, U. Jansson, J. Rosén, Discovery of the Ternary Nanolaminated Compound Nb_2GeC by a Systematic Theoretical-Experimental Approach, *Phys. Rev. Lett.* 109 (3) (2012) 35502.
- [22] C. Hu, H. Zhang, F. Li, Q. Huang, Y. Bao, New Phases' Discovery in MAX Family, *Int. J. Refracat. Met. Hard Mater.* 36 (2013) 300–312.
- [23] M. Husain, N. Rahman, M. Sohail, R. Khan, T. Zaman, R. Neffati, G. Murtaza, A. Azzouz-Rached, A. Khan, DFT-Based Computational Investigations of Structural, Mechanical, Optoelectronics, and Thermoelectric Properties of $InxF_3$ ($X = Be$ and Sr) Ternary Fluoroperovskites Compounds, *Phys. Scr.* 98 (7) (2023) 75905.
- [24] N. Rahman, M. Husain, V. Tirth, A. Alqahtani, H. Alqahtani, T. Al-Mughanam, A. H. Alqahtani, R. Khan, M. Sohail, A.A. Khan, Appealing Perspectives of the Structural, Electronic, Elastic and Optical Properties of $LiRCl_3$ ($R = Be$ and Mg) Halide Perovskites: A DFT Study, *RSC Adv.* 13 (27) (2023) 18934–18945.
- [25] A.A. Rached, I. Ouadha, M. Husain, H. Rached, H. Rebak-Djabri, A. Bentouaf, T. Hadji, N. Sfina, H. Albawali, V. Tirth, First-Principles Calculations to Investigate Physical Properties of Orthorhombic Perovskite YBO_3 ($B = Ti \& Fe$) for High Energy Applications, *RSC Adv.* 13 (7) (2023) 4138–4149.
- [26] J. Wang, Z. Pan, Y. Wang, L. Wang, L. Su, D. Cuiuri, Y. Zhao, H. Li, Evolution of Crystallographic Orientation, Precipitation, Phase Transformation and Mechanical Properties Realized by Enhancing Deposition Current for Dual-Wire Arc Additive Manufactured Ni-Rich NiTi Alloy, *Addit. Manuf.* 34 (2020) 101240.
- [27] W. Yang, X. Jiang, X. Tian, H. Hou, Y. Zhao, Phase-Field Simulation of Nano-A' Precipitates under Irradiation and Dislocations, *J. Mater. Res. Technol.* 22 (2023) 1307–1321.
- [28] Y. Zhao, Y. Sun, H. Hou, Core-Shell Structure Nanoprecipitates in $Fe-XCu-3.0Mn-1.5Ni-1.5Al$ Alloys: A Phase Field Study, *Prog. Nat. Sci. Mater. Int.* 32 (3) (2022) 358–368.
- [29] Y. Yan, K. Zhang, G. Qin, B. Gao, T. Zhang, X. Huang, Y. Zhou, Phase Engineering on MoS_2 to Realize Dielectric Gene Engineering for Enhancing Microwave Absorbing Performance, *Adv. Funct. Mater.* 2316338 (2024).
- [30] X. Long, K. Chong, Y. Su, C. Chang, L. Zhao, Meso-Scale Low-Cycle Fatigue Damage of Polycrystalline Nickel-Based Alloy by Crystal Plasticity Finite Element Method, *Int. J. Fatigue* 175 (2023) 107778.
- [31] Q. Zhu, J. Chen, G. Gou, H. Chen, P. Li, Ameliorated Longitudinal Critically Refracted—Attenuation Velocity Method for Welding Residual Stress Measurement, *J. Mater. Process. Technol.* 246 (2017) 267–275.
- [32] H.B. Zhang, Y.C. Zhou, Y.W. Bao, M.S. Li, Improving the Oxidation Resistance of Ti_3SiC_2 by Forming a $Ti_3SiO_9Al_0.1C_2$ Solid Solution, *Acta Mater.* 52 (12) (2004) 3631–3637.
- [33] I. Salama, T. El-Raghy, M.W. Barsoum, Oxidation of Nb_2AlC and $(Ti, Nb)2AlC$ in Air, *J. Electrochem. Soc.* 150 (3) (2003) C152.
- [34] F.L. Meng, Y.C. Zhou, J.Y. Wang, Strengthening of Ti_2AlC by Substituting Ti with V, *Scr. Mater.* 53 (12) (2005) 1369–1372.
- [35] M.W. Barsoum, T. El-Raghy, M. Ali, Processing and Characterization of Ti_2AlC , Ti_2AlN , and Ti_2AlC 0.5 N 0.5, *Metall. Mater. Trans. A* 31 (2000) 1857–1865.
- [36] G.P. Bel, V. Gauthier-Brunet, C. Tromas, D.S. Synthesis, Characterization, and Intrinsic Hardness of Layered Nanolaminate Ti_3AlC_2 and $Ti_3Al_0.8Sn_0.2C_2$ Solid Solution, *J. Am. Ceram. Soc.* 95 (1) (2012) 102–107.
- [37] Z.-Y. Jiao, T.-X. Wang, S.-H. Ma, Phase Stability, Mechanical Properties and Lattice Thermal Conductivity of Ceramic Material $(Nb_1 - XTix)4AlC_3$ Solid Solutions, *J. Alloys Compd.* 687 (2016) 47–53.
- [38] J. Gu, L. Pan, J. Yang, L. Yu, H. Zhang, W. Zou, C. Xu, C. Hu, T. Qiu, Mechanical Properties and Oxidation Behavior of Ti-Doped Nb_4AlC_3 , *J. Eur. Ceram. Soc.* 36 (4) (2016) 1001–1008.
- [39] S. Lin, Y. Huang, L. Zu, X. Kan, J. Lin, W. Song, P. Tong, X. Zhu, Y. Sun, Alloying Effects on Structural, Magnetic, and Electrical/Thermal Transport Properties in MAX-Phase $Cr_2 - XMgGeC$ ($M = Ti, V, Mn, Fe, and Mo$), *J. Alloys Compd.* 680 (2016) 452–461.
- [40] D. Wan, L. He, L. Zheng, J. Zhang, Y. Bao, Y. Zhou, A New Method to Improve the High-temperature Mechanical Properties of Ti_3SiC_2 by Substituting Ti with Zr, Hf, or Nb, *J. Am. Ceram. Soc.* 93 (6) (2010) 1749–1753.
- [41] H. Gao, R. Benitez, W. Son, R. Arroyave, M. Radovic, Structural, Physical and Mechanical Properties of $Ti_3(Al_1 - XSix)C_2$ Solid Solution with $X = 0 - 1$, *Mater. Sci. Eng. A* 676 (2016) 197–208.
- [42] Elastic and Thermodynamic Properties of New ($Zr_3 - XTix$) AlC_2 MAX - Phase Solid Solutions. 2017, 2017.
- [43] B. Anasori, M. Dahlqvist, J. Halim, E.J. Moon, J. Lu, B.C. Hosler, E.N. Caspi, S. J. May, L. Hultman, P. Eklund, Experimental and Theoretical Characterization of Ordered MAX Phases Mo_2TiAlC_2 and $Mo_2Ti_2AlC_3$, *J. Appl. Phys.* (2015) 118, 9.
- [44] S. Fu, Y. Liu, H. Zhang, S. Grasso, C. Hu, Synthesis and Characterization of High Purity $Mo_2Ti_2AlC_3$ Ceramic, *J. Alloys Compd.* 815 (2020) 152485.
- [45] M. Bendjemai, A.A. Rached, M. Husain, A. Bentouaf, N. Rahman, V. Tirth, A. Alqahtani, A.H. Alqahtani, T. Al-Mughanam, First-Principles Calculations to Investigate Structural, Elastic and Thermodynamic Properties of New M_2ScSnC_2 ($M = V$ or Nb) Quaternary Compounds for 312 MAX Phases, *J. Mater. Res. Technol.* 24 (2023) 3211–3221.
- [46] I. Ouadha, A. Azzouz-Rached, H. Rached, A. Bentouaf, D. Rached, S. Al-Qaisi, Thermomechanical Analysis of the New Ferromagnetic MAX-Phase Compound Mn_2VsC_2 : Insights from DFT Calculations, *Pramana* 97 (2) (2023) 57.
- [47] D. Wang, X.-X. Wang, M.L. Jin, P. He, S. Zhang, Molecular Level Manipulation of Charge Density for Solid-Liquid TENG System by Proton Irradiation, *Nano Energy* 103 (2022) 107819.
- [48] Y. Zhao, B. Zhang, H. Hou, W. Chen, M. Wang, Phase-Field Simulation for the Evolution of Solid/Liquid Interface Front in Directional Solidification Process, *J. Mater. Sci. Technol.* 35 (6) (2019) 1044–1052.
- [49] T. Hadji, H. Khalfoun, H. Rached, Y. Guermat, A. Azzouz-Rached, D. Rached, DFT Study with Different Exchange-Correlation Potentials of Physical Properties of the New Synthesized Alkali-Metal Based Heusler Alloy, *Eur. Phys. J. B* 93 (2020) 1–10.
- [50] A. Bentouaf, H. Rached, A. Azzouz Rached, Theoretical Study of Thermal and Magneto-electronic Properties of Yb_2X ($X = Co$ and Fe) Intermetallic Compounds, *Energy Storage* 5 (6) (2023) e455.
- [51] M. Husain, A. Ullah, A. Alqahtani, V. Tirth, T. Al-Mughanam, A.H. Alqahtani, N. Sfina, K. Briki, H. Albalawi, M.A. Amin, Insight into the Structural, Mechanical and Optoelectronic Properties of Ternary Cubic Barium-Based $BaMCl_3$ ($M = Ag, Cu$) Chloroperovskites Compounds, *Crystals* 13 (1) (2023) 140.
- [52] P. Blaha, K. Schwarz, G.K.H. Madsen, D. Kvasnicka, J. Luitz, Wien2k. An Augment, *PL. Wave+ Local Orbital Progr. Calc. Cryst. Prop.* 60 (1) (2001).
- [53] J.P. Perdew, K. Burke, M. Ernzerhof, Generalized Gradient Approximation Made Simple, *Phys. Rev. Lett.* 77 (18) (1996) 3865.
- [54] A. Azzouz-Rached, M.M.H. Babu, H. Rached, T. Hadji, D. Rached, Prediction of a New Sn-Based MAX Phases for Nuclear Industry Applications: DFT Calculations, *Mater. Today Commun.* 27 (2021) 102233.
- [55] Y. Zhao, Stability of Phase Boundary between $L1_2-Ni_3Al$ Phases: A Phase Field Study, *Intermetallics* 144 (2022) 107528.
- [56] X. Han, C. Zhao, S. Wang, Z. Pan, Z. Jiang, X. Tang, Multifunctional TiO_2/C Nanosheets Derived from 3D Metal-Organic Frameworks for Mild-Temperature-Photothermal-Sonodynamic-Chemodynamic Therapy under Photoacoustic Image Guidance, *J. Colloid Interface Sci.* 621 (2022) 360–373.
- [57] T. Hadji, H. Khalfoun, H. Rached, A. Azzouz-Rached, Ab-Initio Prediction of High TC Half-Metallic Ferrimagnetism in Li-Based Heusler Compounds Mn_2LiZ ($Z = Si, Ge$ and Sn), *Comput. Condens. Matter* 27 (2021) e00557.
- [58] F. Mouhat, F.-X. Couder, Necessary and Sufficient Elastic Stability Conditions in Various Crystal Systems, *Phys. Rev. B* 90 (22) (2014) 224104.

- [59] H.B. Huntington, The Elastic Constants of Crystals, in: Solid State Physics, Vol. 7, Elsevier, 1958, pp. 213–351.
- [60] O.T. Bruhns, The Prandtl-Reuss Equations Revisited, ZAMM-Journal Appl. Math. Mech. Für Angew. Math. Und Mech. 94 (3) (2014) 187–202.
- [61] R. Hill, The Elastic Behaviour of a Crystalline Aggregate, Proc. Phys. Soc. Sect. A 65 (5) (1952) 349.
- [62] V. Kumar, A.K. Shrivastava, V. Jha, Bulk Modulus and Microhardness of Tetrahedral Semiconductors, J. Phys. Chem. Solids 71 (11) (2010) 1513–1520.
- [63] M.N.H. Liton, M. Roknuzzaman, M.A. Helal, M. Kamruzzaman, A. Islam, K. Ostrikov, M.K.R. Khan, Electronic, Mechanical, Optical and Photocatalytic Properties of Perovskite RbSr₂Nb₃O₁₀ Compound, J. Alloys Compd. 867 (2021) 159077.
- [64] Pugh, S. F. XCII. Relations between the Elastic Moduli and the Plastic Properties of Polycrystalline Pure Metals. London, Edinburgh, Dublin Philos. Mag. J. Sci. 1954, 45 (367), 823–843.
- [65] A. Savin, H. Flad, J. Flad, H. Preuss, H.G. von Schnering, Zur Bindung in Carbosilanen, Angew. Chemie 104 (2) (1992) 185–186.
- [66] X. Jiang, J. Zhao, X. Jiang, Correlation between Hardness and Elastic Moduli of the Covalent Crystals, Comput. Mater. Sci. 50 (7) (2011) 2287–2290.
- [67] M. Sokol, V. Natu, S. Kota, M.W. Barsoum, On the Chemical Diversity of the MAX Phases, Trends Chem. 1 (2) (2019) 210–223.
- [68] H.M. Ledbetter, Elastic Properties of Zinc: A Compilation and a Review, J. Phys. Chem. Ref. Data 6 (4) (1977) 1181–1203.
- [69] J. Wang, Y. Zhou, T. Liao, Z. Lin, First-Principles Prediction of Low Shear-Strain Resistance of Al₃BC₃: A Metal Borocarbide Containing Short Linear BC₂ Units, Appl. Phys. Lett. 89 (2) (2006).
- [70] O.L. Anderson, A Simplified Method for Calculating the Debye Temperature from Elastic Constants, J. Phys. Chem. Solids 24 (7) (1963) 909–917.
- [71] M.E. Fine, L.D. Brown, H.L. Marcus, Elastic Constants versus Melting Temperature in Metals, Scr. Metall. 18 (9) (1984) 951–956.
- [72] G. Qin, A. Huang, Y. Liu, H. Wang, Z. Qin, X. Jiang, J. Zhao, J. Hu, M. Hu, High-Throughput Computational Evaluation of Lattice Thermal Conductivity Using an Optimized Slack Model, Mater. Adv. 3 (17) (2022) 6826–6830.
- [73] C. Dhakal, S. Aryal, R. Sakidja, W.-Y. Ching, Approximate Lattice Thermal Conductivity of MAX Phases at High Temperature, J. Eur. Ceram. Soc. 35 (12) (2015) 3203–3212.
- [74] D.R. Clarke, S.R. Phillipot, Thermal Barrier Coating Materials, Mater. Today 8 (6) (2005) 22–29.
- [75] D.R. Clarke, Materials Selection Guidelines for Low Thermal Conductivity Thermal Barrier Coatings, Surf. Coatings Technol. 163 (2003) 67–74.
- [76] Y. Liu, V.R. Cooper, B. Wang, H. Xiang, Q. Li, Y. Gao, J. Yang, Y. Zhou, B. Liu, Discovery of AB O₃ Perovskites as Thermal Barrier Coatings through High-Throughput First Principles Calculations, Mater. Res. Lett. 7 (4) (2019) 145–151.
- [77] A. Otero-de-la-Roza, D. Abbasi-Pérez, V. Luña, Gibbs2, A New Version of the Quasiharmonic Model Code. II. Models for Solid-State Thermodynamics, Features and Implementation, Comput. Phys. Commun. 182 (10) (2011) 2232–2248.